Engineered Science
DOI: https://dx.doi.org/10.30919/es1830

Broadband Microstrip Antenna Array Design for Wireless Communication in the 2.3–2.5 GHz Band

Kymbat Kopbay,[1] Madiyar Nurgaliyev,[1,*] Nursultan Meirambekuly,[1,2] Ahmet Saymbetov,[1] Askhat Bolatbek,[1] Batyrbek Zholamanov,[1] Nursultan Koshkarbay[1] and Sayat Orynbassar[1]

Abstract

This paper presents the design, simulation, and experimental validation of a planar broadband microstrip patch antenna array with passive beam tilt capability, optimized for operation in the 2.3–2.5 GHz ISM band. A 2×2 rectangular patch array was developed on a low-cost FR-4 substrate, employing a quarter-wave transformer (QWT)-based corporate feeding network with asymmetrical feedline lengths to introduce phase shifts. This configuration achieves a fixed downward beam tilt of approximately 30° without the use of active components or complex geometries. The fabricated antenna demonstrates a measured impedance bandwidth of 202 MHz (2.34–2.542 GHz), an S_11 parameter of approximately -20 dB, and a half-power beamwidth (HPBW) of 60° in the E-plane. Full-wave simulations in HFSS and outdoor experimental measurements confirm the intended radiation behavior and impedance characteristics. The proposed antenna design offers a compelling combination of bandwidth, gain, mechanical simplicity, and directional control, making it well-suited for industrial IoT nodes, ceiling-mounted access points, and wireless sensor networks.

Keywords: Broadband antenna array; Passive beam tilt; Microstrip patch antenna; Quarter-wave transformer; 2.4 GHz ISM band; FR-4 substrate.
Received: 09 September 2025; Revised: 15 October 2025; Accepted: 22 October 2025
Article type: Research article.

1. Introduction

Under present conditions of pervasive wireless connectivity, the 2.4 GHz industrial, scientific, and medical (ISM) band stands out as one of the most densely occupied frequency domains.[1] Its global availability and compatibility with popular wireless technologies such as Wi-Fi, Zigbee, Bluetooth, and a broad range of IoT protocols have led to substantial spectral crowding.[2] As the number of connected devices continues to increase, issues such as interference, multipath fading, and congestion pose significant challenges to ensuring reliable data transmission in complex environments.[3] To meet these challenges, the development of broadband antennas that can maintain efficient performance across a wider spectrum without complex or expensive structures has become essential.[4] Such antennas facilitate the coexistence of multiple wireless standards and help mitigate performance degradation caused by environmental fluctuations. Additionally, broadband microstrip antennas have been widely adopted in real-world deployments such as wireless access points, industrial IoT networks, and vehicle-to-infrastructure systems due to their ability to support multiple overlapping communication standards with high efficiency. This real-world relevance further underscores the need for research into compact and cost-effective wideband solutions.

Microstrip patch antennas (MPAs) are well-known recognized for their thin profile, planar structure, ease of integration, and manufacturability.[5] However, conventional MPAs typically exhibit inherently narrow impedance bandwidths (often 2–3% on FR-4) and are highly sensitive to structural perturbations, which limits their adaptability in broadband and interference-prone conditions.[6] To enhance the operational bandwidth and radiation efficiency of MPAs, researchers have employed a variety of design innovations.[7-11] These include techniques such as slot incorporation,[12] the use of parasitic elements,[13] elevation via air gaps,[14] and sophisticated feeding strategies like proximity coupling,[15]

[1]*Faculty of Physics and Technology, Al-Farabi Kazakh National University, 71 Al-Farabi, Almaty, 050040, Kazakhstan*
[2]*Khoja Akhmet Yassawi International Kazakh-Turkish University, 29 Sattarhanov Street, Turkistan, 161200, Kazakhstan*
[*]*Email:* nurgaliyev.madiyar@kaznu.kz (Madiyar Nurgaliyev)

coplanar waveguides,[16] and quarter-wave transformer (QWT)[17] implementations. Such methods are aimed at expanding the impedance bandwidth while preserving a compact form factor suitable for integration.

Several recent studies have explored diverse approaches to antenna design in the 2.4 GHz ISM band, targeting enhancements in impedance bandwidth, physical compactness, and compatibility with low-cost substrates such as FR-4.[18–25] For example, in,[18] a floating patch configuration with through-wire feeding and an integrated air gap achieved a fractional bandwidth (FBW) exceeding 10% and a radiation efficiency above 95%. While the design maintains a relatively simple structure and avoids the use of exotic materials, some mechanical assembly steps—such as the implementation of the air gap and coaxial probe feed extend beyond conventional PCB fabrication processes. A compact L-shaped microstrip antenna tailored for IoT applications was presented in,[19] attaining a 5.8% FBW with a realized gain of 2.09 dBi within a highly constrained footprint. Similarly,[20] demonstrated that the performance limitations typically associated with FR-4 substrates can be overcome through careful geometrical optimization, as shown in a filter-integrated wideband antenna design. In,[21] a dual-polarized structure employing differential-pair arms enhanced both isolation and bandwidth, providing a viable option for MIMO systems. Meanwhile, unconventional geometries such as octagonal patches[22] and L-fed configurations[23] have been employed to improve bandwidth and coverage under various usage conditions, including on-body environments. Although these works show progress, most FR-4 based antennas achieve only 3–6% FBW.

While these studies emphasize wideband performance and integration simplicity, few address the ability to shape or tilt the radiation pattern—particularly in a passive manner. Beam tilting is essential in practical applications where the antenna must cover downward zones, such as human-occupied spaces or industrial floors. Several efforts have investigated passive beam tilting, though often at the expense of bandwidth. In,[24] a parasitic-element-loaded patch array achieved a tilt of over 30° in the X–Z plane at 2.5 GHz using a truncated ground plane, though its design exhibited FBW of only 4%. A similar concept was explored in,[25] where a series-fed 2×1 array achieved beam tilt along a single axis within the 2.4–2.45 GHz band. Fixed-angle beam-switching in 2×2 arrays was demonstrated in[26] using 3 dB couplers, producing ±20° tilt at 2.4 GHz. In another recent work,[27] a dielectric resonator antenna with a passive beam-steering mechanism was introduced for the 2.4 GHz band. By leveraging the asymmetrical placement of dielectric elements, the de-sign achieved single-axis beam tilting in the E-plane without requiring any active components. The approach was experimentally validated and demonstrated good directivity with moderate bandwidth. Despite their benefits, most of these techniques suffer from limited impedance bandwidth, dependence on complex or non-planar structures, or lack of scalability for conventional PCB manufacturing. Therefore, a combined solution that offers both enhanced bandwidth and passive beam steering in a single-layer, low-cost FR-4 structure remains largely unexplored in literature.

In contrast, the present work introduces a compact, wideband 2×2 microstrip patch antenna array that achieves both a broad impedance bandwidth and a passive beam tilt of 30° in the E-plane. The array employs a simple rectangular patch design fabricated on cost-effective FR-4 substrate, with inter-element spacing and feedline geometry carefully optimized to balance performance and manufacturability. Bandwidth enhancement is achieved through the incorporation of QWT within a parallel corporate feeding network, which improves impedance matching and effectively reduces reflection losses over a wide frequency range. Importantly, a passive phase shift is introduced via asymmetric central feedline lengths between the upper and lower patch elements. This results in a directional beam tilt, confirmed both by full-wave simulations and analytical array factor modeling.

The tilted radiation pattern is particularly advantageous in overhead deployment scenarios, *e.g.*, ceiling or wall-mounted installations, where coverage of downward-oriented regions is required. The outdoor free-space measurements demonstrated that proposed antenna achieved an impedance bandwidth of 202 MHz (2.34–2.542GHz, with S11 < –25 dB) and a peak gain of 7.49 dBi. These characteristics, combined with the planar structure, low cost, and fully passive operation, make the proposed antenna a strong candidate for integration into a variety of contemporary communication systems. It is particularly well suited for applications requiring reliable directional coverage and high energy efficiency, while avoiding the added complexity and cost of active beamforming circuitry. Potential use cases include wireless mesh networks, high-density indoor access points, antenna elements for distributed MIMO systems, and infrastructure nodes for smart city and IoT deployments. The antenna's capability to deliver fixed, predictable coverage with minimal hardware overhead makes it an attractive option for scalable and cost-efficient next-generation wireless networks, including private 5G/6G systems and advanced signal acquisition platforms.

2. Materials and methods

This section outlines the design methodology and theoretical principles underpinning the proposed 2×2 microstrip patch antenna array (PAA) with fixed beam tilt. The design process includes patch dimensioning, impedance matching using QWT, and the implementation of a passive feed network with asymmetrical line lengths to induce beam tilting. All structures were realized on standard FR-4 substrate (ε_r = 4.4, h = 1.6 mm), optimized for the 2.3–2.5 GHz ISM band.

2.1 Materials and sample preparation

MPA's have become a popular choice in contemporary wireless systems due to their compact size, straightforward manufacturing process, and seamless integration with electronic circuitry. In this work, the patch antenna was designed based on the classical microstrip antenna theory, as described in.[28,29] The operating frequencyf_{op} for a rectangular patch operating in the dominant TM_{10}mode can be estimated using the following Eq. (1):

$$f_{op} = \frac{c}{2L\sqrt{\varepsilon_{eff}}} \tag{1}$$

where c is the speed of light in vacuum ($\approx 3 \times 10^8\ m/s$), L is the effective length of the patch, ε_{eff} is the effective dielectric constant of the substrate. The dimensions of the patch antenna - specifically its width and length - play a crucial role in determining its resonant frequency, radiation characteristics, and impedance matching performance. These parameters directly affect the antenna's efficiency and overall behavior. The width $\boldsymbol{W}$ of the patch can be determined using the following Eq. (2):

$$W = \frac{c}{2f_r}\sqrt{\frac{2}{\varepsilon_r+1}} \tag{2}$$

where $\boldsymbol{\varepsilon_r}$ is the relative dielectric constant of the substrate material. A wide range of substrate materials can be used in the design of MPAs, including options like FR-4, Rogers RT/Duroid, and Teflon, with relative permittivity values typically ranging from 2.2 to 12. The selection of a suitable substrate depends on multiple factors such as cost-effectiveness, thermal stability, dielectric losses, and other physical properties. In this study, FR-4 epoxy was chosen as the substrate material, featuring a dielectric constant of $\boldsymbol{\varepsilon_r}$ =4.4 and a thickness of h=1.6 mm.

In microstrip antenna analysis, the effective dielectric constant $\boldsymbol{\varepsilon_{eff}}$is introduced to represent the combined effect of the substrate and the surrounding air on the propagation of electromagnetic waves. Since the fields are not entirely confined within the dielectric material but also extend into the air, the actual wave propagation occurs in a medium with an effective permittivity that lies between the permittivity of the substrate and that of free space. This equation describes how the effective dielectric constant impacts the wave propagation speed within the substrate. A higher effective permittivity reduces the guided wavelength, leading to more compact patch dimensions but potentially higher dielectric losses. Understanding this relationship is crucial for balancing antenna size and efficiency Eq. (3).

$$\varepsilon_{eff} = \frac{\varepsilon_r+1}{2} + \frac{\varepsilon_r-1}{2}\left(1+12\frac{h}{W}\right)^{-\frac{1}{2}} \tag{3}$$

In MPA's, the fringing field effect arises because the electromagnetic fields at the edges of the patch do not abruptly terminate but rather extend slightly into the surrounding air. This phenomenon effectively increases the electrical length of the patch, altering its resonant behavior. To account for this, an additional length component, denoted as ΔL is introduced into the design process. The extension due to the fringing fields can be estimated using the following empirical Eq. (4):

$$\Delta L = 0.412h\frac{\left(\varepsilon_{ref}+0.3\right)\left(\frac{W}{h}+0.264\right)}{\left(\varepsilon_{ref}-0.258\right)\left(\frac{W}{h}+0.8\right)} \tag{4}$$

The actual physical length of the patch is Eq. (5):

$$L = \frac{c}{2f_{op}\sqrt{\varepsilon_{eff}}} - 2\Delta L \tag{5}$$

These equations ensure accurate dimensioning for resonance at 2.4GHz, taking into consideration the dielectric loading and field fringing effects.

2.2 Quarter-wave transformer design

In microstrip antenna design, the method used to deliver electromagnetic energy from the transmission line to the radiating element plays a vital role in determining key performance aspects, including impedance matching, radiation pattern, operating frequency, and polarization. In this study, a direct edge-fed microstrip configuration was employed due to its straightforward design and ease of fabrication. This approach involves directly connecting a microstrip transmission line to the edge of the rectangular patch. Regardless of the feeding type, achieving effective impedance matching is critical, as it minimizes reflected signals and standing waves while maximizing power transfer efficiency. This can be accomplished by carefully adjusting the dimensions, particularly the width and length of the feed line. The first step involves determining the input impedance of the patch antenna using the following relationship Eq. (6):

$$Z_{in} = 90 * \frac{{\varepsilon_r}^2}{\varepsilon_r - 1}\left(\frac{L}{W}\right)^2 \tag{6}$$

A QWT is utilized to match the impedance between the standard 50 Ω microstrip feed line and the input impedance of the patch antenna. The impedance of $\boldsymbol{Z_{QWT}}$ is given by Eq. (7):

$$Z_{QWT} = \sqrt{Z_{in}Z_{feed}} \tag{7}$$

Where $\boldsymbol{Z_{in}}$in is the input impedance of the patch, $Z_{feed}$is the impedance of the feed line (commonly 50Ω). The QWT

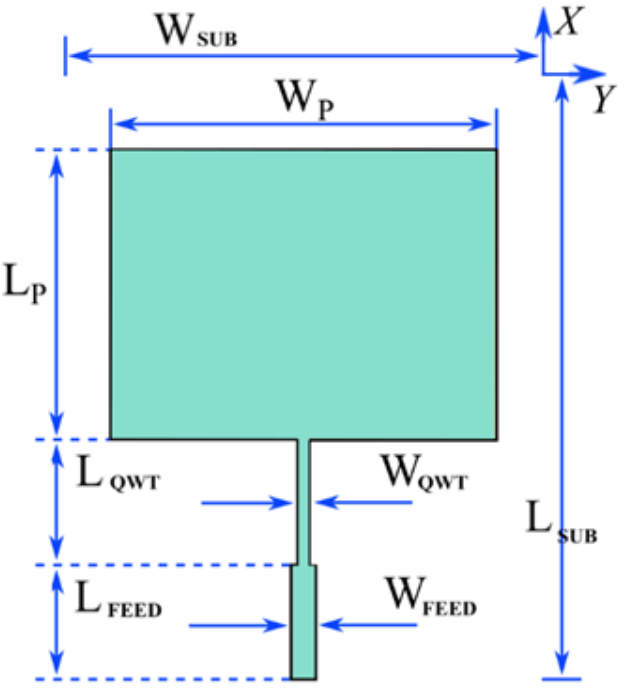

Fig. 1: Single patch antenna design.

Table 1: The dimension parameters of rectangular single patch antenna.

Parameters	W_p	L_p	W_{QWT}	L_{QWT}	W_{feed}	L_{feed}	W_{sub}	L_{sub}	h
Values (mm)	37.10	27.60	1.20	15.00	2.98	15.00	48.00	65.40	1.60

section of the microstrip line has a physical length corresponding to one-quarter of the guided wavelength, *i.e.*, $\boldsymbol{\lambda/4}$. Its width is determined using conventional transmission line design equations, which take into account the desired characteristic impedance $\boldsymbol{Z_0}$, the substrate thickness h, and the relative dielectric constant $\boldsymbol{\varepsilon_r}$ of the material Eq. (8):[30]

$$Z_0 = \begin{cases} \frac{60}{\sqrt{\varepsilon_r}} \ln\left(\frac{8h}{W} + \frac{W}{4h}\right), & \frac{W}{h} < 1 \\ \frac{120\pi}{\sqrt{\varepsilon_r}\left(1.393 + \frac{W}{h} + \frac{2}{3}\ln\left(\frac{W}{h} + 1.444\right)\right)}, & \frac{W}{h} > 1 \end{cases} \quad (8)$$

Fig. 1 illustrates the top view of a single rectangular patch antenna, including the feed line and QWT. The key geometrical parameters of the antenna structure are labeled for clarity. Table 1 summarizes the corresponding dimensions of each design element used in the antenna model.

2.3 Array configuration and layout

Three distinct configurations - a standalone patch, a linear dual-element array, and a planar four-element (2×2) array were designed to investigate the influence of element coupling, spatial arrangement, and feed topology on antenna performance. All structures were fabricated on a common substrate and simulated under identical frequency constraints to ensure fair comparison.

The single patch antenna (SPA) was designed as a reference model to evaluate the intrinsic characteristics of the radiating element. The calculated patch dimensions ensure resonance at the target frequency while minimizing the influence of surface waves and edge effects. This design exhibits moderate gain and a quasi-omnidirectional azimuth pattern, serving as the foundation for further array expansion.

To increase directivity and suppress radiation in undesired directions, two identical patch elements were arranged in a collinear format along the y-axis, as shown in Fig. 2(a). The inter-element gap was set to approximately half the free-space wavelength to balance mutual coupling and radiation efficiency. A corporate feeding network was used to distribute the input signal evenly, incorporating a quarter-wave impedance transformer at each branch point to ensure consistent phase and amplitude delivery. This configuration leads to a more concentrated main lobe in the broadside direction and improves overall gain performance.

To further enhance the antenna gain, bandwidth and achieve a downward beam tilt via passive phase control, a compact planar 2×2 patch array was designed, as illustrated in Fig. 2(b). The four patch elements were symmetrically arranged with inter-element spacings of 0.38λ₀ and 0.47λ₀ along the X and Y axes, respectively. The distance between patches does not exceed 0.5λ₀ to avoid grating lobes while maintaining sufficient coupling to enable field superposition.[31]

The feed network was extended into a balanced parallel four-branch corporate structure, incorporating two stages of power division using QWTs to maintain uniform phase

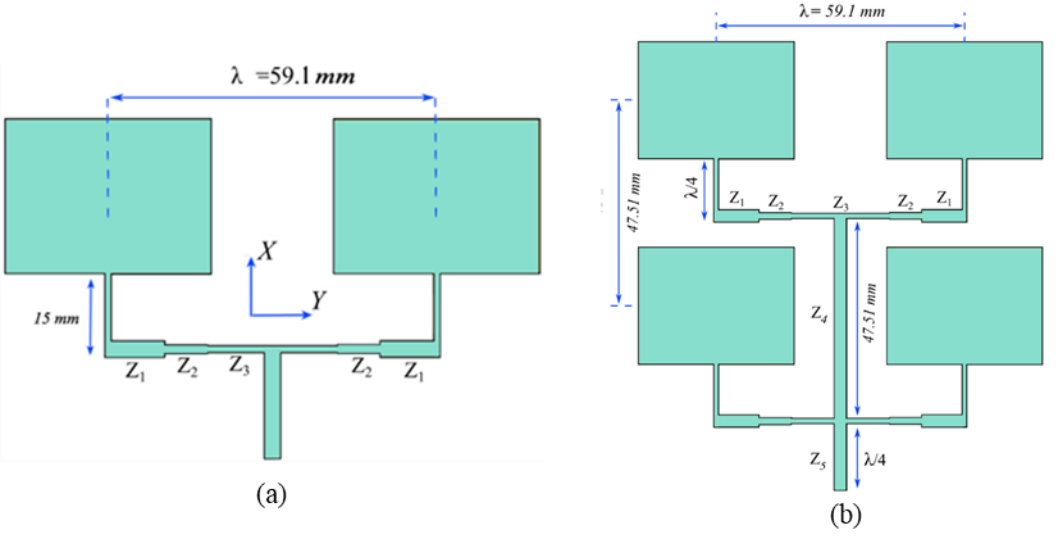

Fig. 2: The proposed design of a) two elements, b) four element PAA.

Table 2: Design parameters of the feed matching network.

Parameters	W_{z1}	L_{z1}	W_{z2}	L_{z2}	W_{z3}	L_{z3}	W_{z4}	L_{z4}	W_{z5}	L_{z5}
Values(mm)	2.98	10.80	1.54	7.63	1.20	23.42	2.98	47.51	2.98	15.99

distribution. This configuration provides increased bandwidth and gain characteristics, reduced sidelobe levels, and improved directivity compared to the linear array counterpart. Additionally, the symmetric architecture of the feed system facilitates seamless array expansion and integration into modular or reconfigurable antenna platforms.

The entire feeding system was implemented on a single-layer FR-4 substrate using planar microstrip lines, which simplifies fabrication and ensures compatibility with standard PCB manufacturing. Quarter-wavelength microstrip sections were employed at each branching level to match impedance transitions. The characteristic impedance at each segment was calculated using the geometric mean of the input and output impedances, as defined by Eq. (9):

$$Z_{match} = \sqrt{Z_1 Z_2} \tag{9}$$

where Z_1 and Z_2 are the impedances of adjacent microstrip segments. This approach minimizes signal reflection and ensures maximum power transfer to each radiating element, preserving phase coherence across the array. The detailed physical dimensions of each feed segment are presented in Table 2.

2.4 Array factor

The observed downward tilt of the main radiation lobe in the proposed four-element patch array is attributed to a controlled phase offset between the radiating elements. This intentional phase difference is achieved through unequal central feedline length connecting the antenna patches and can be analyzed analytically using the concept of the Array Factor (AF).

To begin the analysis, we consider the phase delay Δφ introduced by a microstrip line of length Δl on a dielectric substrate. This delay, expressed in radians, is defined as Eq. (10):[32]

$$\Delta\varphi = \frac{2\pi\Delta l}{\lambda_g} \tag{10}$$

where, Δl is the difference in feedline length and λ_g is the guided wavelength. This equation is a fundamental concept in wave physics and underpins array theory in antenna engineering. The guided wavelength is calculated by the following Eq. (11):

$$\lambda_g = \frac{\lambda_0}{\sqrt{\varepsilon_{reff}}} \tag{11}$$

The AF is a key theoretical construct used in the analysis of antenna arrays. It represents the interference pattern created by the superposition of waves radiated from multiple antenna elements, considering only their geometrical arrangement and relative excitation phases. It does not include the individual element radiation patterns. Instead, it isolates the effect of array geometry and phase differences on the overall directional behavior. It provides an analytical approximation of the array's radiation characteristics and is especially valuable in the design phase for predicting main lobe directions and sidelobe levels.

For a 2-dimensional M×N planar antenna array, the general expression for AF(θ) is Eq. (12):

$$AF(\theta) \sum_{m=0}^{M-1}\sum_{n=0}^{N-1} e^{j(mkd_x sin\theta cos\phi + nkd_y sin\theta sin\phi + \psi_{mn})} \tag{12}$$

where, θ and ϕ are the elevation and azimuth angle, respectively; $\boldsymbol{k} = \frac{2\pi}{\lambda_g}$ is wave number based on the guided

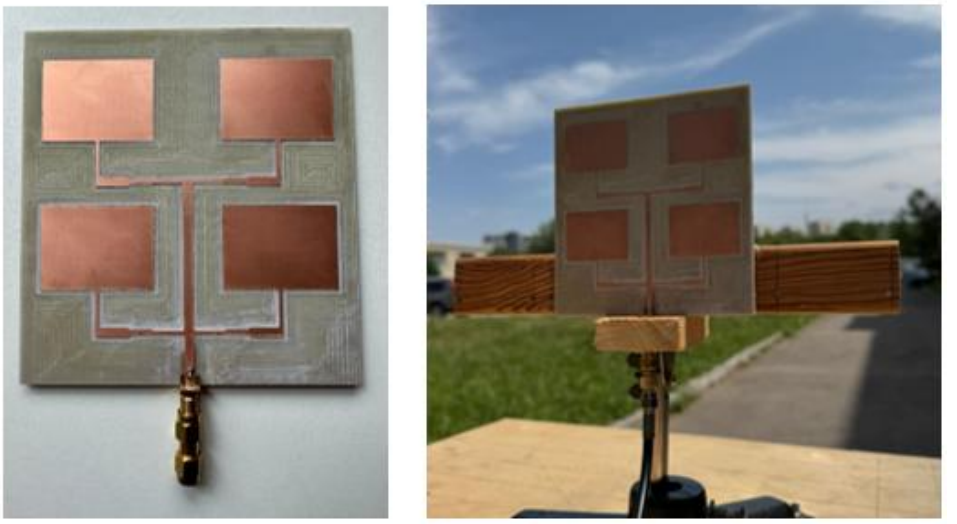

Fig. 3: Manufactured prototype of the four-element PAA.

Fig. 4: The outdoor measurement set up.

wavelength λ_g; d_x and d_y are inter-element spacing along X and Y axes; ψ_mn is phase excitation of element position (m, n).

In this configuration, a 2x2 square patch antenna array is employed. The array elements are equally spaces in both X and Y directions, with vertical spacing $d_x = 47.51mm$ and horizontal spacing $d_y = 59.1mm$. The feedline structure introduces a vertical phase delay, the top patches are fed through longer vertical microstrip lines, resulting in a phase lag compared to the bottom patches. This results in a noticeable tilt of the main beam along the X-axis (in the plane ϕ=0). The tilt arises due to constructive interference between the top and bottom patch elements, which generates directional radiation in the X-Z plane (commonly referred to as the E-plane), orthogonal to the imposed phase gradient.

3. Results and discussion

This section presents a comprehensive comparison of the simulated performance of the single-element, two-element array, and four-element array MPA configurations, along with experimental validation of the four-element configuration conducted in an outdoor free-space environment. All antennas were designed to operate in the 2.4 GHz ISM band and simulated using the Ansys HFSS 2023 R1 full-wave electromagnetic solver. The substrate material employed in all designs was FR-4, with a relative permittivity $\boldsymbol{\varepsilon_r}$ of 4.4 and a standard loss tangent suitable for low-cost fabrication.

The simulation-based evaluation includes key performance metrics such as the reflection coefficient $\boldsymbol{S_{11}}$, voltage standing wave ratio (VSWR), and far-field radiation characteristics, including both 2D and 3D gain patterns. For experimental verification, a four-element array prototype shown in Fig. 3, was fabricated and tested using a Keysight FieldFox vector network analyzer (VNA). The VNA enabled the measurement of S-parameters, VSWR, and far-field radiation pattern under realistic outdoor conditions with the technique of the reference antenna.

Fig. 4 presents the experimental outdoor measurement setup used for the far-field validation of the four-element PAA. The antenna under test (AUT) is mounted on a height-

adjustable tripod at a fixed location, while the reference antenna is placed at a known distance aligned along the boresight axis. This configuration enables precise measurement of the radiation characteristics in free-space conditions. The VNA (Keysight FieldFox) provides live monitoring of the reflection coefficient and gain behavior across the targeted frequency band. The measurement setup employed a 2.5-meter separation between the AUT and the reference antenna, with boresight alignment accuracy within ±2°. Measurements were conducted in an open outdoor area with minimal surrounding reflectors to reduce multipath interference.

The simulated and measured S_{11} parameters for the single-, dual-, and four-element antenna configurations is presented in Fig. 5. The single patch (blue curve) shows a narrow resonant bandwidth with a deep minimum at 2.4 GHz, reaching -47 dB, and a -10 dB bandwidth ranging from 2.37 GHz to 2.43 GHz (≈60 MHz). The dual-element design (orange curve) extends this range to 2.37–2.45 GHz (≈80 MHz), while maintaining a return loss of -45 dB at resonance. The most significant improvement is observed in the four-element PAA. The simulated $\boldsymbol{S_{11}}$ (green curve) indicates a broad -10 dB impedance bandwidth from 2.276 GHz to 2.547 GHz, amounting to 271 MHz (≈11.3% fractional bandwidth). The measured $\boldsymbol{S_{11}}$ of the fabricated four-element prototype (dashed red line) closely aligns with the simulated response, showing a well-defined resonance between 2.340 GHz and 2.542 GHz, corresponding to a bandwidth of 202 MHz. A minimum reflection coefficient value of approximately < -20 dB is observed at 2.43GHz, indicating good impedance matching and low reflection.

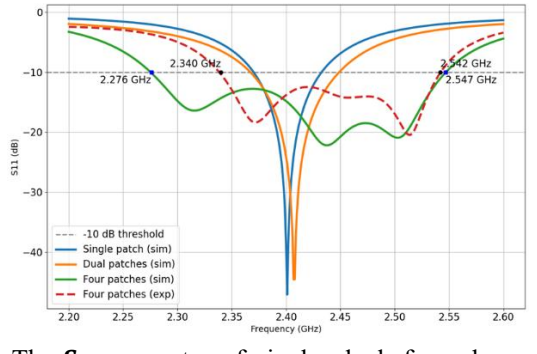

Fig. 5: The $\boldsymbol{S_{11}}$ parameter of single, dual, four element patch antennas.

This high level of agreement between simulation and measurement confirms the reliability of the design methodology and validates the effectiveness of the QWT in improving impedance matching. The enhancement in bandwidth with array size is attributed to strong coupling and field superposition between adjacent patches, which improves energy distribution and reduces reflection across a broader frequency range. However, minor differences between simulated and measured results are observed, which can be attributed to practical implementation factors. First, SMA connectors and coaxial cables used during measurements introduce additional insertion loss and small impedance mismatches that are not modeled in the HFSS simulations. Second, fabrication tolerances, such as slight deviations in substrate thickness, copper etching, and dielectric constant ($\boldsymbol{\varepsilon_r}$) of FR-4, affect the resonance and impedance matching. Even a ±0.1 mm variation in microstrip line width can lead to noticeable changes in $\boldsymbol{S_{11}}$ characteristics. Additionally, FR-4 exhibits variations in dielectric properties across frequency and manufacturing batches, contributing to discrepancies between ideal simulations and real-world performance. Finally, environmental influences, including ground reflections and surrounding objects during outdoor measurements, can slightly alter the far-field response. Despite these factors, the overall correlation between simulated and measured data remains strong, validating the robustness of the proposed design. Fabrication tolerances included ±0.1 mm in substrate thickness, ±0.05 mm in microstrip trace width, and SMA connector losses of approximately 0.2 dB, which together explain the small deviations between measured and simulated results.

In Fig. 6, we can observe the VSWR characteristics for the simulated and manufactured patch antenna configurations. As expected, the single patch (blue curve) exhibits the highest VSWR values outside the narrow resonance band, dropping to ~1 at 2.4 GHz, which corresponds to its resonant point. However, the VSWR rapidly increases beyond ±30 MHz from the center frequency, indicating a relatively narrow operational bandwidth. The dual-element configuration (orange curve) shows improved impedance matching over a wider frequency range, maintaining a VSWR < 2 between approximately 2.37 GHz and 2.45 GHz. This suggests more efficient power transfer and reduced signal reflection due to better field distribution and element interaction.

The four-element PAA (green curve) demonstrates the most desirable performance. The simulated VSWR remains below 2 from 2.27 GHz to 2.55 GHz and achieves a near-ideal value of >1 at the resonant frequency of 2.40 GHz. The measured data (dashed red curve) for the fabricated prototype further confirms these findings, with the experimental VSWR remaining below 2 across most of the operating band, demonstrating even better impedance matching performance than the simulated results.

The proposed array achieves high efficiency despite being implemented on a low-cost FR-4 substrate. HFSS simulations indicate a radiation efficiency of approximately 78–80% across the operating band. Using the measured realized gain and simulated directivity, the estimated total efficiency of the fabricated antenna is about 82%, with negligible mismatch loss due to excellent impedance matching ($|\boldsymbol{S_{11}}|$ < –25 dB). This performance demonstrates that the feed network and design optimization effectively minimize losses, making the

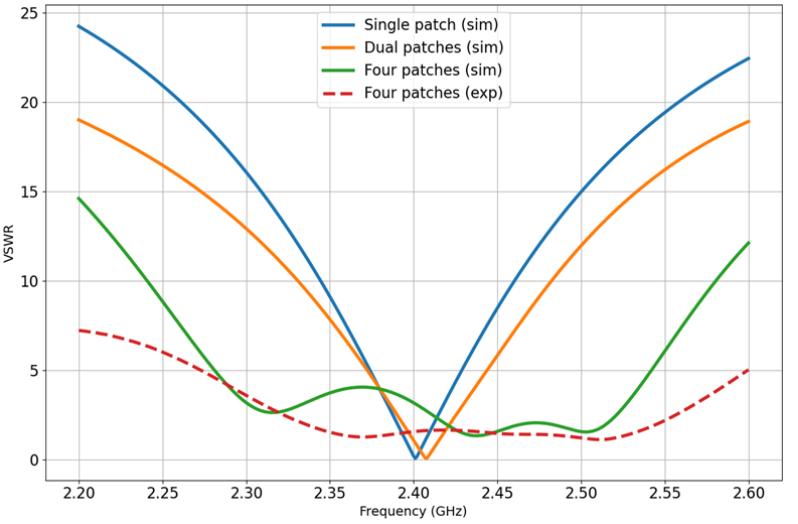

Fig. 6: The VSWR of single, dual, four element patch antennas.

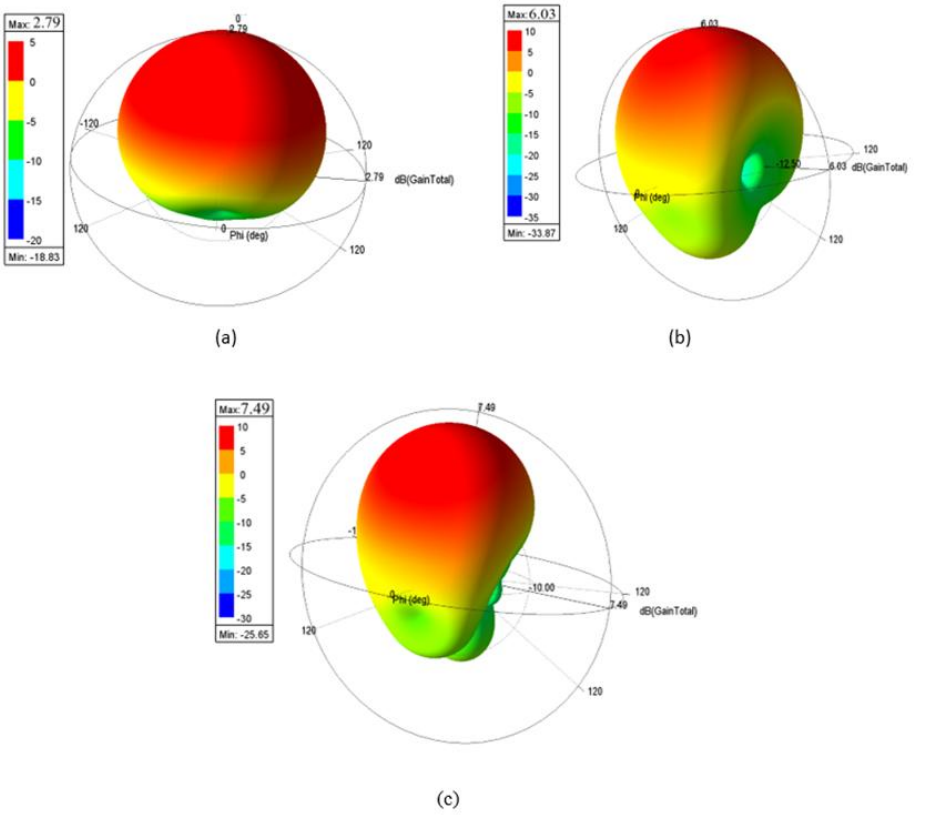

Fig. 7: The 3D radiation pattern of a) single, b) dual, c) four element patch antennas.

antenna highly suitable for practical wireless applications.

Fig. 7 illustrates the 3D far-field radiation patterns for the (a) single, (b) dual-, and (c) four-element MPA configurations at the resonant frequency of 2.4 GHz. In Fig. 7(a), the single patch exhibits a quasi-omnidirectional radiation pattern in the simulated free-space environment, with maximum gain of 2.79 dBi and relatively uniform radiation in all directions. The pattern is nearly spherical, as expected from an isolated rectangular patch with no directional constraints, and is suitable for applications requiring wide-area coverage but not high directivity. It should be noted that in the experimental setup, some back radiation may be slightly suppressed due to reflections from the mounting structure and surrounding environment; however, this does not affect the main lobe behavior or overall design analysis. Fig. 7(b) shows the dual-patch configuration, where the main lobe becomes more focused along the broadside direction due to constructive interference between the two radiating elements. The peak gain increases to 6.03 dBi, and the backward radiation is notably suppressed, forming a more directional beam compared to the single element. This improvement is primarily attributed to enhanced current distribution and

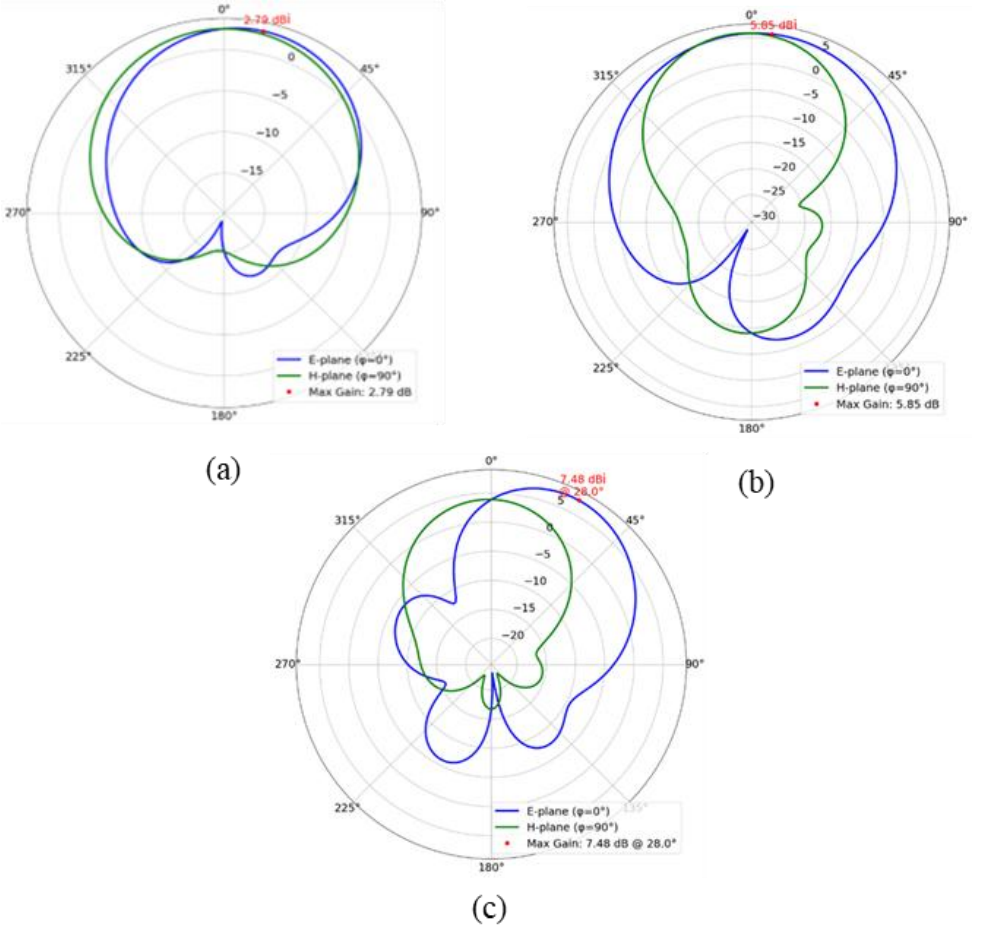

Fig. 8: The 2D radiation pattern of a) single, b) dual, c) four element patch antennas.

mutual coupling. In Fig. 7(c), the four-element array achieves the most pronounced directive behavior, with a maximum gain of 7.49 dBi. The radiation lobe of the four-element array remains well-formed and symmetrical despite the higher directivity, indicating a uniform power distribution across the elements. The absence of grating lobes or pronounced sidelobes demonstrates that the element spacing and feed network are carefully optimized to suppress unwanted radiation modes. This is particularly important in multi-element configurations, as improper spacing often leads to secondary lobes that degrade coverage quality and increase interference. The smooth transition of the main lobe without irregular ripples further confirms efficient impedance matching and coherent phase alignment among elements. These characteristics ensure predictable radiation behavior and make the design suitable for controlled coverage in dense wireless environments.

The simulated 2D radiation patterns in the E-plane (φ = 0°, blue) and H-plane (φ = 90°, green) demonstrate the evolution of the antenna's directivity and gain with increasing array complexity.

For the single-element configuration (Fig. 8(a)), the radiation pattern remains broad and nearly symmetric, with a maximum gain of 2.79 dBi. The shape of both E- and H-plane patterns is indicative of quasi-omnidirectional behavior, making this design suitable for applications where uniform spatial coverage is desired. In the dual-element configuration (Fig. 8(b)), the E-plane narrows significantly, resulting in increased directivity along the boresight. The gain improves to 5.85 dBi, and while the H-plane shows minor distortion due to mutual coupling, the overall pattern integrity is preserved. These results confirm enhanced constructive interference and improved field concentration in the main lobe direction. The four-element configuration (Fig. 8(a)) exhibits a pronounced directional behavior with a clearly visible downward beam tilt of approximately 28° in the E-plane. The main lobe reaches a peak gain of 7.48 dBi, enabled by the intentional phase offset introduced through asymmetrical feedline lengths implemented within a parallel corporate feeding network using QWTs. This configuration offers high directionality and is well suited for fixed installations requiring downward coverage, such as ceiling-mounted wireless sensors or access points. The E-plane narrowing and H-plane stability indicate efficient phase alignment across the array, ensuring minimal sidelobe distortion. The downward tilt observed in Fig. 8(c) corresponds closely with the theoretical predictions, reinforcing that beam steering is achieved without active elements.

Fig. 9 compares the normalized gain patterns obtained through array factor analysis and full-wave HFSS simulations

for different central feedline lengths in the four-element patch array. The orange curve represents the theoretical array factor model for a 2×2 configuration with a Y-axis phase shift. The dashed curves correspond to simulated gain responses using varying feedline lengths: 45 mm, 47.51 mm (nominal design), and 55 mm. As expected, the position of the main lobe is sensitive to the phase difference introduced by the central feedline length. When the central line is shortened to 45 mm, the beam direction shifts slightly upward, while a longer feedline of 55 mm results in a more pronounced downward tilt and additional ripple in the side lobes. This behavior highlights the importance of precise feedline length tuning to maintain phase coherence across the array.

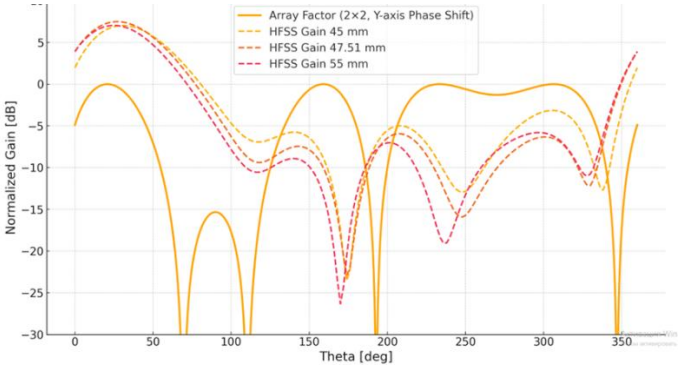

Fig. 9: Normalized gain for different central feedline lengths compared to the theoretical AF.

Overall, the excellent correspondence between the simulated gain patterns and the analytical array factor validates the phase delay strategy used in the design. It confirms that the radiation pattern of the antenna can be accurately predicted and engineered by controlling microstrip line geometry alone, enabling low-cost, passive beam steering without active circuitry.

The full-wave simulated 3D radiation pattern of the four-element PAA is shown in Fig. 10, including the beam tilt effect as implemented through asymmetrical feedline design. The visualization highlights the integration of electromagnetic field distribution with the radiation lobe, offering insight into how the structural configuration of the antenna impacts its radiative behavior. The main lobe is clearly tilted downward by approximately 28°, confirming the intended passive beam steering mechanism. This tilt arises from the unequal electrical path lengths between the upper and lower patch elements in the array, which induces a controlled phase shift. Notably, the shape of the radiation lobe remains well-formed and symmetrical despite the tilt, indicating uniform power distribution among the radiating elements. The gain distribution within the lobe is smooth, and the absence of grating lobes or side maxima reflects the effective array spacing and impedance matching strategy.

This result directly supports the theoretical AF predictions and validates the simulation findings presented in Fig. 7 and 8, demonstrating that precise beam direction control can be achieved in a fully passive and planar microstrip implementation.

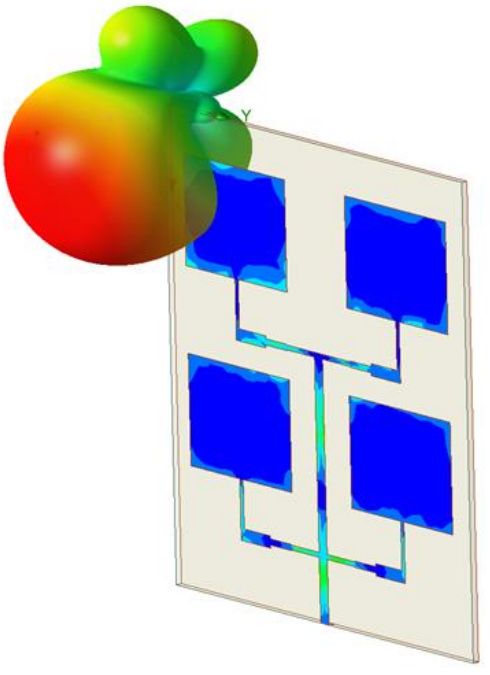

Fig. 10: Simulated 3D radiation pattern of the four-element array exhibiting a 28° beam tilt.

To evaluate the directional characteristics of the fabricated antenna in real-world conditions, Fig. 11 presents the experimentally measured 2D radiation patterns along the horizontal cut (H-plane) for two antenna orientations. The blue curve corresponds to the antenna mounted in a vertical (upright) position, while the red curve represents measurements taken with the antenna physically tilted upward by 30°. It is important to note that the original measured values were obtained directly from the Keysight measurement system and were not normalized, thereby preserving the actual signal strength for comparison and analysis.

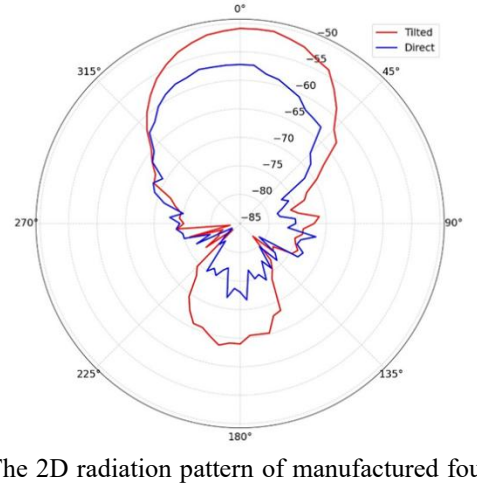

Fig. 11: The 2D radiation pattern of manufactured four element patch antennas at a tilt of 30 degrees (red) and without tilt (blue) in dB at 2.43GHz.

Table 3: Comparative analysis of existing 2.4 GHz antenna solutions with bandwidth, gain, and beam tilt characteristics.

Year	Ref.	Type	Substrate	f_c(GHz)	R_L(dB)	BW(%)	G(dBi)	Beam Tilt(°)	Experimental validation
2022	[18]	Floating patch with through-wire feed	Rogers-4003C	2.4	- 30.00	10.41	9.63	No	Yes
2023	[19]	Compact L-shaped patch	Rogers 5880	2.4	- 30.00	5.8	2.09	No	Yes
2019	[23]	L-shape fed patch for WBAN	FR-4	2.45	- 23.15	4.9	5.09	No	Yes
2023	[24]	Parasitic patch, tilted ground	FR-4	2.5	≈-30.00	4	2.3	> 30	Yes
2024	[25]	Series-fed, honeycomb-shaped	PLA and copper tape	2.4-2.45	- 20.15	≈ 4	7.72	≈ 30	Yes
2020	[26]	2 × 2 series-fed, 3 dB/90 couplers	NH9450	2.4	> -20	≈ 3.5	9.5	± 20	Yes
2024	[27]	Hemispherical liquid antenna with metaball	FR-4, liquid materials	2.4	> -20	≈ 12	5.5	≈ 60	Yes
2025	This work	2x2 patch array with QWT	FR-4	2.4	-20	≈8.5	7.49(sim)	30	Yes

A pronounced increase in signal strength is observed at the 30° elevation when the antenna is tilted upward, confirming that the main lobe of the array is inherently directed downward when the antenna is in its normal upright position. In this orientation, the main beam is tilted approximately 28°–30° downward, so a portion of the radiated energy is directed below the horizontal plane rather than toward the reference antenna during measurement. As a result, the received power in the upright position is lower because the measurement system is aligned along the boresight axis, not along the actual direction of maximum radiation.

When the antenna is physically rotated upward by 30°, its main lobe is realigned toward the reference antenna, causing the measured power to increase significantly. This observation confirms the presence of a controlled downward beam tilt, predicted as 28° in the full-wave HFSS simulations (presented in Fig. 8) and AF analysis and validated as approximately 30° in measurements. The small difference of about 2° can be attributed to fabrication tolerances, connector effects, and environmental conditions during outdoor testing. The strong correlation between simulated and measured results validates the accuracy of the asymmetrical feedline design in achieving passive phase control.

This feature is particularly beneficial for overhead deployment scenarios such as ceiling-mounted access points or sensor nodes, where controlled coverage of user or workspace areas below is required. The strong agreement between simulated and measured patterns confirms the reliability of the electromagnetic design and the practical viability of the antenna for wideband directional applications.

In Table 3 we provide a comparative overview of the proposed four-element PAA against recent state-of-the-art designs operating in the 2.4 GHz ISM band. The comparison highlights key performance metrics, including BW, gain, beam tilt angle, substrate type, and the presence of experimental validation.

Among the listed works, designs employing high-performance substrates such as Rogers 4003C[19] and Rogers 5880[20] have achieved notable radiation efficiency. However, these improvements come at the cost of higher material prices and manufacturing complexity, which restricts their feasibility for large-scale or cost-sensitive applications. The study in,[24] which employed FR-4, achieved a 4.9% bandwidth and moderate gain of 5.09 dBi. This value is nearly half of what our proposed antenna provides in terms of bandwidth, despite using the same substrate type. This clearly demonstrates the efficiency of the implemented impedance-matching strategy in our design. These works did not incorporate beam tilting, thereby limiting their directional functionality. Beam tilting was addressed in works such as,[25-28] often through structural modifications like tilted grounds, honeycomb substrates, 3 dB couplers, or liquid metastructures. While these approaches demonstrated directional control (tilt angles ranging from 30° to ±60°), they either introduced complexity (*e.g.*, non-planar structures, specialized materials) or suffered from limited bandwidth (typically ≤ 4%). In contrast, this work achieves a bandwidth of 202 MHz (≈8.5%), a peak gain of 7.49 dBi, and a 30° downward beam tilt, all while using a standard, low-cost FR-4 substrate and a compact, planar layout. Importantly, the design is fully passive, relying on an asymmetrical feed network to induce the required phase shift, and is validated experimentally with excellent agreement between simulated and measured results.

Compared to recent literature, the proposed antenna offers a favorable combination of broad bandwidth, high gain, mechanical simplicity, and directional control within a fully

passive, single-layer planar structure. These features make it highly suitable for a wide range of modern wireless communication applications, particularly where directional beam control and passive implementation are essential. Potential applications include compact base stations, distributed antenna systems and indoor/outdoor access points in industrial and commercial environments. The antenna's passive beam tilting capability is especially advantageous in scenarios requiring fixed coverage shaping, such as in smart buildings, factory automation, and massive IoT deployments, where spatial filtering, interference mitigation, and energy-efficiency are critical. Furthermore, its compatibility with low-cost manufacturing and scalability makes it attractive for integration into large-scale MIMO systems, 5G/6G small cells, and emerging signal-processing platforms that rely on stable and directive antenna elements.

4. Conclusion

This work presents the comprehensive development and validation of a wideband microstrip PAA with passive downward beam tilt, designed for the 2.3–2.5 GHz ISM band. A planar 2×2 configuration was implemented using a low-cost FR-4 substrate and a QWT-based parallel corporate feed network. By introducing deliberate asymmetry in the central feedline lengths, a fixed phase offset was achieved between array elements, enabling passive beam steering without the use of active components or complex geometries. The design methodology was supported by full-wave electromagnetic simulations and analytical array factor modeling. Parametric analysis across single-, dual-, and four-element configurations demonstrated a clear progression in bandwidth, gain, and beam directionality. The fabricated four-element prototype exhibited a measured bandwidth of 202 MHz (8.5%), a peak gain of 7.49 dBi, and a downward main beam tilt of 30°, with excellent agreement between simulated and experimental results.

The proposed antenna demonstrates a wide bandwidth, directional radiation, and structural simplicity, making it suitable for applications such as distributed antenna systems, wireless sensor networks, smart environments, IoT nodes. Future research may focus on expanding the array size, integrating reconfigurable or switchable tilt angles, and evaluating performance under dynamic multipath conditions. The presented approach provides a scalable and manufacturable solution for modern wireless infrastructure requiring both spectral efficiency and spatial coverage control. Moreover, the presented design can be scaled to larger arrays or adapted for future 5G/6G deployments by incorporating reconfigurable phase-shifting networks or tunable substrates, enabling dynamic control of beam direction and improved spectral utilization.

Acknowledgments

This research has been funded by the Science Committee of the Ministry of Science and Higher Education of the Republic of Kazakhstan (Grant AP19678552).

Conflict of Interest

There is no conflict of interest.

Supporting Information

Not applicable.

CRedit Statement

Kymbat Kopbay: Conceptualization, Supervision, Project administration, Methodology, Writing - Original draft, **Madiyar Nurgaliyev:** Conceptualization, Methodology, Investigation, Data curation, Writing - Review & editing, **Nursultan Meirambekuly:** Investigation, Data curation, Formal analysis, Validation, **Ahmet Saymbetov:** Investigation, Supervision, Funding acquisition, **Askhat Bolatbek:** Software, Visualization, Experimental work. **Batyrbek Zholamanov:** Investigation, Statistical analysis, Preparation of figures and tables, **Nursultan Koshkarbay:** Writing - Review & editing, Literature search, Editing for technical accuracy, **Sayat Orynbassar:** Resources, Supervision, Visualization, Writing - Review & editing.

References

[1] A. A. Eltholth, Improved spectrum coexistence in 2.4 GHz ISM band using optimized chaotic frequency hopping for Wi-Fi and bluetooth signals, *Sensors*, 2023, **23**, 5183, doi: 10.3390/s23115183.

[2] Z. M. Kidane, W. Dargie, Cross-technology interference: detection, avoidance, and coexistence mechanisms in the ISM bands, *CCF Transactions on Pervasive Computing and Interaction*, 2025, **7**, 356-375, doi: 10.1007/s42486-025-00185-0.

[3] J.-H. Lee, S.-J. Kho, U.-J. Jang, Y.-S. Hong, An improved method of avoiding RF congestion in indoor environments, *Procedia Engineering*, 2016, **154**, 223-228, doi: 10.1016/j.proeng.2016.07.455.

[4] N. Parveen, K. Abdullah, K. Badron, Y. Javed, Z. I. Khan, Coexistence in wireless networks: challenges and opportunities, *Telecom*, 2025, **6**, 23, doi: 10.3390/telecom6020023.

[5] M. S. Yahya, S. Soeung, S. K. Abdul Rahim, U. Musa, S. S. Ba Hashwan, Z. Yunusa, S. A. Hamzah, LoRa microstrip patch antenna: a comprehensive review, *Alexandria Engineering Journal*, 2024, **103**, 197-221, doi: 10.1016/j.aej.2024.06.017.

[6] M. U. Khan, M. S. Sharawi, R. Mittra, Microstrip patch antenna miniaturisation techniques: a review, *IET Microwaves, Antennas & Propagation*, 2015, **9**, 913-922, doi: 10.1049/iet-map.2014.0602.

[7] S. K. Noor, M. Jusoh, T. Sabapathy, A. H. Rambe, H. Vettikalladi, A. M. Albishi, M. Himdi, A patch antenna with enhanced gain and bandwidth for sub-6 GHz and sub-7 GHz 5G wireless applications, *Electronics*, 2023, **12**, 2555, doi: 10.3390/electronics12122555.

[8] P. A. Kashyap, K. Sarmah, I. Dakua, S. Baruah, Gain and bandwidth enhancement of slotted microstrip antenna using metallic nanofilms for WLAN applications, *Journal of King Saud*

University - Science, 2023, **35**, 102374, doi: 10.1016/j.jksus.2022.102374.
[9] Younes, Siraj, Kaoutar Saidi Alaoui, and Foshi Jaouad, Metamaterials for Performance Enhancement of THz Patch Antenna for 6G and Biomedical Applications, *The International Conference on Artificial Intelligence and Smart Environment*, Springer, Cham, Lecture Notes in Networks and Systems, 2024, 1397, doi: 10.1007/978-3-031-90921-4_8.
[10] Halgurd N. Awl, Yadgar I. Abdulkarim, Lianwen Deng, Mehmet Bakır, Fahmi F. Muhammadsharif, Muharrem Karaaslan, Emin Unal and Heng Luo, Bandwidth Improvement in Bow-Tie Microstrip Antennas: The Effect of Substrate Type and Design Dimensions, *Applied Science*, 2020, **10**(2), 504, doi: 10.3390/app10020504.
[11] F. Karami, H. Boutayeb, A. Amn-E-Elahi, A. Ghayekhloo, L. Talbi, Developing broadband microstrip patch antennas fed by SIW feeding network for spatially low cross-polarization situation, *Sensors*, 2022, **22**, 3268, doi: 10.3390/s22093268.
[12] X.-K. Zhang, X.-Y. Wang, S.-C. Tang, J.-X. Chen, Y.-J. Yang, A wideband filtering dielectric patch antenna with reconfigurable bandwidth using dual-slot feeding scheme, *IEEE Access*, 2021, **9**, 96345-96352.
[13] L. C. Paul, H. K. Saha, T. Rani, M. Z. Mahmud, T. K. Roy, W.-S. Lee, An omni-directional wideband patch antenna with parasitic elements for sub-6 GHz band applications, *International Journal of Antennas and Propagation*, 2022, **2022**, 9645280, doi: 10.1155/2022/9645280.
[14] A. M. Chowdhury, S. Alam, M. A. Alim, Ultra-wideband THz microstrip patch antenna with enhanced performance through air-hole optimization, *26th International Conference on Computer and Information Technology (ICCIT)*, Cox's Bazar, Bangladesh December 13-15, 2023, 1-5, doi: 10.1109/ICCIT60459.2023.10440973.
[15] A. K. Awasthi, C. D. Simpson, S. Kolpuke, T. D. Luong, J.-B. Yan, D. Taylor, S. P. Gogineni, Ultra-wideband patch antenna array with an inclined proximity coupled feed for small unmanned aircraft RADAR applications, *IEEE Open Journal of Antennas and Propagation*, 2021, **2**, 1079-1086.
[16] M. S. Jameel, Y. S. Mezaal, D. C. Atilla, Miniaturized coplanar waveguide-fed UWB antenna for wireless applications, *Symmetry*, 2023, **15**, 633, doi: 10.3390/sym15030633.
[17] J. Y. Lee, M. Zhu, K. Yang, Y. C. Lee, I. I. Idrus, Wide-slot tri-band patch antenna fed by quarter wave transformer for biomedical applications, *IEEE MTT-S International Microwave Biomedical Conference (IMBioC)*, 2022, Suzhou, China, May 16-18, 2022, 232-235, doi: 10.1109/IMBioC52515.2022.9790123.
[18] M. d. Fernandez, D. Herraiz, David Herraiz, A. Alomainy, A. Belenguer, Design of a Wide-Bandwidth, High-Gain and Easy-to-Manufacture 2.4 GHz Floating Patch Antenna Fed with the Through-Wire Technique, *Applied Science*, 2022, **12**, 12925, doi: 10.3390/app122412925.
[19] M. F. Zambak, S. S. Al-Bawri, M. Jusoh, A. H. Rambe, H. Vettikalladi, A. M. Albishi, M. Himdi, A compact 2.4 GHz L-shaped microstrip patch antenna for ISM-band Internet of Things (IoT) applications, *Electronics*, 2023, **12**, 2149, doi: 10.3390/electronics12092149.
[20] Y. I. A. Al-Yasir, M. K. Alkhafaji, H. A. Alhamadani, N. Ojaroudi Parchin, I. Elfergani, A. L. Saleh, J. Rodriguez, R. A. Abd-Alhameed, A new and compact wide-band microstrip filter-antenna design for 2.4 GHz ISM band and 4G applications, *Electronics*, 2020, **9**, 1084, doi: 10.3390/electronics9071084.
[21] Y. Li, L. Wei, K. Wang, H. Cai, Z. Chen, Low-profile wideband dual-polarized patch antenna based on differential-paired multi-mode arms, *Electronics*, 2023, **12**, 2604, doi: 10.3390/electronics12122604.
[22] N. N. Tawfeeq, S. D. Mahmood, Simulation study of microstrip antenna for 2.45 GHz applications based on octagon shaped, *Materials Today: Proceedings*, 2021, **42**, 2448-2456, doi: 10.1016/j.matpr.2020.12.560.
[23] C.-E. Guan, T. Fujimoto, Design of a wideband L-shape fed microstrip patch antenna backed by conductor plane for medical body area network, *Electronics*, 2020, **9**, 21, doi: 10.3390/electronics9010021.
[24] N. A. F. Mohd Zainudin, M. N. Osman, T. Sabapathy, M. Jusoh, M. N. Mohd Yasin, M. K. A Rahim, Low-profile and wider-angle beam tilting parasitic array resonator antenna with optimized deflected ground plane on FR-4 substrate, *Micromachines*, 2023, **14**, 834, doi: 10.3390/mi14040834.
[25] S. Noghanian, Y.-H. Chang, P. Guerron, R. Dahle, Series-fed microstrip patch antenna array with additive-manufactured foldable honeycomb-shaped substrate, *Micromachines*, 2024, **15**, 1449, doi: 10.3390/mi15121449.
[26] H. Nawaz, I. Tekin, Ten switched-beams with 2 × 2 series-fed 2.4 GHz array antenna and a simple beam-switching network, *International Journal of RF and Microwave Computer-Aided Engineering*, 2020, **30**(6), e22184, doi: 10.1002/mmce.22184.
[27] V. R. Gudivada, Y. Huang, E. L. Bennett, A passive beamforming hemispherical liquid antenna using a simple metal ball, *IET Microwaves, Antennas & Propagation*, 2024, **18**, 681-690, doi: 10.1049/mia2.12497.
[28] Balanis, A. Constantine, Antenna theory, *Analysis and design*, John wiley & sons, 2016, 1104, ISBN- 978-1-118-64206-1.
[29] Garg, Ramesh, Microstrip antenna design handbook, *Technology & Engineering*, Artech house, 2001, 845, ISBN-0890065136.
[30] Pozar, M. David, Microwave engineering: theory and techniques, *Microwave Engineering*, John wiley & sons, 2011, 752, ISBN 978-0-470-63155-3.
[31] Delos, Peter, Bob Broughton, and Jon Kraft, Phased array antenna patterns—part 2: grating lobes and beam squint, *Analog Dialogue*, 2020, 54, 1-4.
[32] M. I. Nabeel, K. Singh, M. U. Afzal, D. N. Thalakotuna, K. P. Esselle, Dual-band passive beam steering antenna technologies for satellite communication and modern wireless systems: a review, *Sensors*, 2024, **24**, 6144, doi: 10.3390/s24186144.